Proceedings of the Canadian Society for Mechanical Engineering International Congress 2021
CSME Congress 2021
June 27-30, 2021, Charlottetown, PE, Canada

Drag Reduction on a Square Back Ahmed Body Using a Simple Flap

Naseeb Ahmed Siddiqui[1], Martin Agelin-Chaab[2]

[1,2] Faculty of Engineering and Applied Science, Ontario Tech University, 2000 Simcoe Street, North, Oshawa, ON, L1G 0C5, Canada

*Naseeb.siddiqui@ontariotechu.net

Abstract— A simple passive flap device has been applied over a square back Ahmed body. A parametric study varying the angle of implementation, length, width, and ground clearance has been carried out to calculate the optimum size of the flap and ground clearance. It was found that a flap with 135mm length and 389mm width at a 10° implementation angle provides 8.8% of drag reduction. Furthermore, the same flap enhanced this reduction to 12.5% at 25mm ground clearance. The study is conducted using Ansys Fluent at a Reynolds number of 7.8 x 10^5 while employing the SST k-omega model. Vortex identification methods namely Q-criterion and Lambda-2 criterion have been used to further elaborate the change in flow topology due to this passive flap device. However, a detailed study is underway to precisely define the nature of such modifications.

Keywords-Ahmed body, Passive device, drag reduction techniques, vortex identification, Q-criterion, Lambda-2 criterion

I. INTRODUCTION *(HEADING 1)*

The large low-pressure region dominates a square back Ahmed body at the rear. It confers the boundary of the separated wake. The base drag is a direct function of this low-pressure recirculation region, and its modification is significant to produce road vehicles that consume less fuel. Hence, crucial insights are necessary to understand the physics of the recirculation region to develop robust flow control methods.

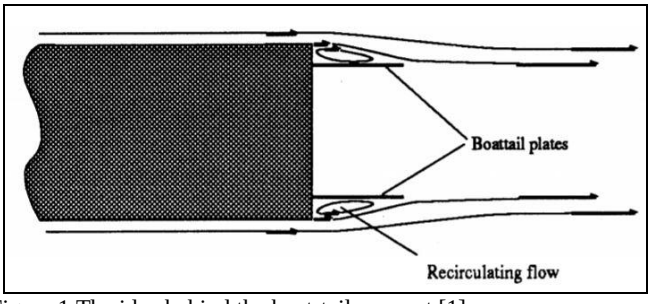

Figure 1 The idea behind the boat-tail concept [1]

However, NASA [1] conducted a full-scale investigation using flat plates forming an aerodynamic boat-tail configuration shown in Figur 1. Such a mechanism diverts the flow inward, which reduces the base area, and the recirculation flow is trapped above and below the flat plates. A total of 4 different plates was found to provide a drag reduction of 10% when implemented offset to the edges by 0.06w (where w is the width of the model) with a plate length of 0.36w. Such a boat-tail increases the pressure at the base area; however, this analysis did not comment on the quantification of the recirculation region after the boat-tail. Khalighi et al., (2001) [2] used the same boat-tail mechanism as [1] on a square back Ahmed body. However, the same configuration narrows the overall aspect ratio of the recirculation region without changing the length. Moreover, it provides a 20% drag reduction to the base model, which is almost twice achieved by [1] on the Truck/trailer model. The same mechanism of the flat plate, when applied to the General motor model, provides a drag reduction of 14% [3]. A similar mechanism is used by [4], who achieved base drag reduction while applying deflectors over a square back vehicle. They found the best performing configuration when both horizontal and vertical deflectors are used at a 20° angle, with the size of the vertical deflector remains 2/3 model height. They reported that reducing the size of the separated region simultaneously dampens the oscillations created due to longitudinal vortices [4]. Such a modification reduced the wake region in the vertical direction, shortens the separated wake, and lessened the base drag by around 10%. These flow features differ significantly with the fastback Ahmed body, and hence, the selection of the flow control devices is critical as per the rear geometry. For example, one documented by [5] implementing small flaps around the edges of the 30° slant Ahmed body surface offered 25% drag reduction. Others like [6]–[8] investigated the small flaps at different fastback Ahmed bodies. Though a square back long hauls MAN TGX truck was simulated by [9] with three different flap shapes; nonetheless, they did not discuss the effect of the recirculation region on drag reduction.

The literature clarifies that, on a square back Ahmed model, the use of flap/deflectors/plate as passive devices

remains understudied. In the applications so far, only small flaps/deflectors have been used. Therefore, the objective of this paper is to study the effect of a single flap installed at the blunt edge of the square back Ahmed body to observe the impact of the length, width, and the ground effect of the flap on the base drag.

2. Vehicle Model and Passive Device Details

The square back Ahmed body provides a giant recirculation bubble at the rear, which is the primary cause of high base drag. The overall dimension of the square back model is 1044mm in length, 288mm in height, 389mm in width, and ground clearance is 50mm as shown in Figure 2, which are the actual dimensions reported by [10]. The main flow features and drag coefficients are well documented, providing enough data to validate the results.

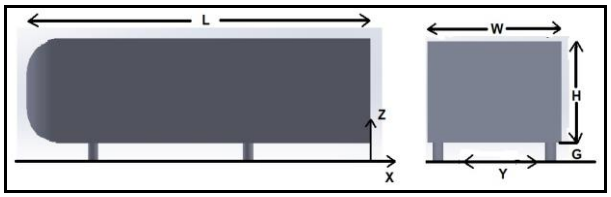

Figure 2 Specification of the Square back Ahmed body. Where Length (L) = 1044mm, Width (W) = 389mm, Height (H) = 288mm and Ground clearance (G) = 50mm. The origin of the axis begins at the bottom of the blunt end.

The proposed flap has a rectangular shape with an aspect ratio (Width/Length) of 2.146 installed at the rear of a square back Ahmed body at the ground clearance of 50mm shown in Figure 3. In the first phase, the angle of implementation is changed to find the angle for the maximum drag reduction. It was found to be 10° at a 2.146 aspect ratio. In the second phase, to see the effect of flap length, it was varied at a fixed width of 389mm. Hence, a further reduction is achieved at flap length 135mm that results in a flap aspect ratio of 2.88. In the third phase at this specific aspect ratio, the effect of flap width was analyzed that reported increased drag except for the original width of 389mm, with the same aspect ratio of 2.88. In the fourth phase, however, such an aspect ratio is then studied for the ground height effect by varying the ground clearance from 25mm to 100mm, where 50mm clearance was the constant in all the simulations. All such information is tabulated in Table 1 for more clarification.

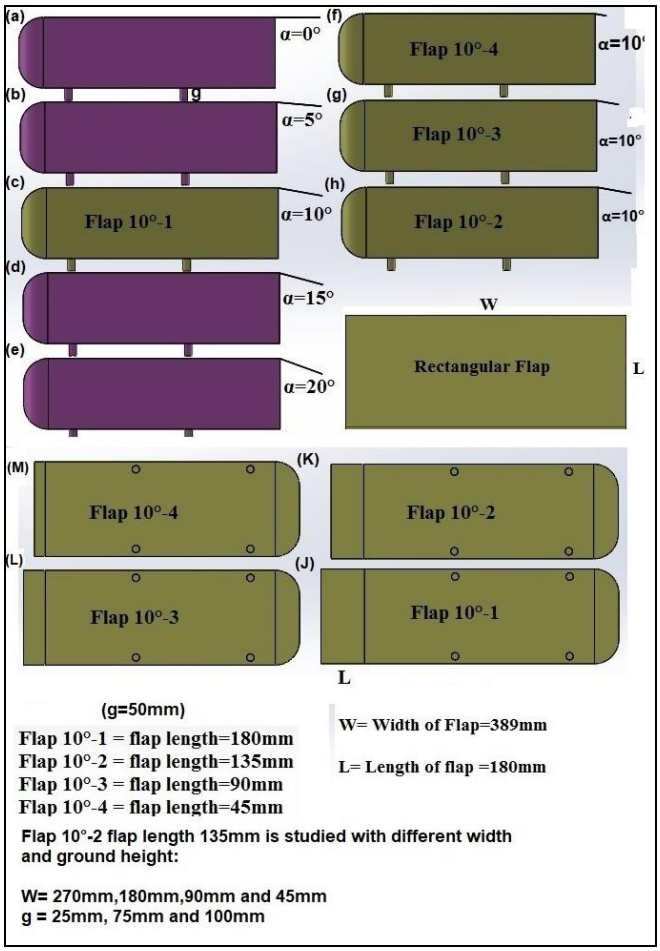

Figure 3 The details of the square back model with flap. The initial investigation was done with a rectangular flap of length 180mm and width 389mm for the flap angle α = 0°- 20° shown from(a) to (e). After the optimum angle is found to be α = 10°, the length of the flap is changed at this particular angle to discover the optimum length (f) to (h). The front and plan view of these modified flap corresponds to (c) & (J) = flap length 180mm, (h) & (K) = flap length 135mm, (g) & (L) = flap length 90mm and (f) & (M) = flap length 45mm. The flap 135mm at 10° provides the maximum drag reduction and hence, it is varied for width(W) and ground height (g).

TABLE 1 THE SPECIFICATION OF THE PASSIVE FLAP DEVICE (REFER TO FIGURE 3)

SPECIFICATION	FLAP LENGTH (MM)	FLAP WIDTH (MM)	ASPECT RATIO OF THE FLAP (W/L)	FLAP ANGLE (°)	GROUND CLEARANCE (MM)
THE FIRST PHASE- ANGLE VARIATION					
FLAP 0°	180	389	2.1	0	50
FLAP 5°	180	389		5	
FLAP 10°-1	180	389		10	
FLAP 15°	180	389		15	
FLAP 20°	180	389		20	
SECOND PHASE – LENGTH VARIATION					
FLAP 10°-2	135	389	2.8	10	50
FLAP 10°-3	90	389	4.3	10	
FLAP 10°-4	45	389	8.6	10	
THIRD PHASE – WIDTH VARIATION					
FLAP 10°-2	135	270	2	10	50
FLAP 10°-2	135	180	1.3	10	
FLAP 10°-2	135	90	0.6	10	
FLAP 10°-2	135	45	0.3	10	
FOURTH PHASE- GROUND CLEARANCE VARIATION					
FLAP 10°-2	135	389	2.1	10	25
FLAP 10°-2	135	389		10	75
FLAP 10°-2	135	389		10	100

3. SIMULATION DETAILS

3.1 MATHEMATICAL MODEL

The time-dependent solution of complex bodies down to extracting small-scale phenomena using the Navier Stokes Equations is not practical with the current computational skills [11]. The Reynolds Averaged Navier-stokes (RANS) equations are used for a time-averaged flow field, so the velocity is not instantaneous. In the aerodynamic community, the RANS is almost established as an incompressible model (Kim et al., 1998). The simulation was performed using the commercial software, Ansys Fluent. The governing equations for the steady-state flow conditions are used to calculate the flow around the Ahmed body. Through Reynolds decomposition, the instantaneous Navier-Stokes equations are converted into Reynolds-Averaged Navier-Stokes equations for incompressible turbulent flow. The steady-state RANS equations for mass and momentum are:

Continuity

$$\frac{\partial}{\partial x_i}(\overline{\rho u_i}) = 0 \qquad \textit{Equation 1}$$

Momentum

$$\frac{\partial}{\partial x_j}\left(\overline{\rho u_i u_j}\right) = -\frac{\partial \bar{p}}{\partial x_i} + \frac{\partial}{\partial x_j}\left[\mu\left(\frac{\partial \overline{u_i}}{\partial x_j} + \frac{\partial \overline{u_j}}{\partial x_i} - \frac{2}{3}\partial_{ij}\frac{\partial \overline{u_l}}{\partial x_l}\right)\right] + \frac{\partial}{\partial x_j}\left(-\rho\overline{u_i' u_j'}\right)$$

Equation 2

Here $\bar{\rho}$ is the mean density, $\bar{p}$ is the mean pressure, μ the molecular viscosity and $-\rho\overline{u_i' u_j'}$ are the Reynolds stresses.

3.2 TURBULENCE MODEL

The RANS equations govern the transport of the average flow quantities, but for that, it has to bring additional terms into the equations. There are different closure models to find out the values of these additional terms. In the current study, the Shear stress transport (SST) k-omega model has been used. The SST k-omega model is a blend of k- ω and K-ϵ and is used due to its proven accuracy for a wide range of flows dominated by boundary layer behavior. In this model, k- ω is applied to the inner region of the boundary layer and K-ϵ at the outer region. The SST k-omega model has inspired other models also [11], [13]–[15].

The equations of models are as follows [16], [17]:

$$\frac{\partial(\rho k)}{\partial t} + \frac{\partial(\rho u_j k)}{\partial x_j} = \rho P - \beta\rho\omega k + \frac{\partial\left((\mu+\sigma_k\mu_t)\frac{\partial k}{\partial x_j}\right)}{\partial x_j}$$

Equation 3

$$\frac{\partial(\rho\omega)}{\partial t} + \frac{\partial(\rho u_j \omega)}{\partial x_j} = \frac{\gamma}{v_t}P - \beta\rho\omega^2 + \frac{\partial\left((\mu+\sigma_\omega\mu_t)\frac{\partial\omega}{\partial x_j}\right)}{\partial x_j} + 2(1-F_1)\frac{\rho\sigma_{\omega 2}}{\omega}\frac{\partial k}{\partial x_j}\frac{\partial\omega}{\partial x_j}$$

Equation 4

$$P = \tau_{ij}\frac{\partial u_i}{\partial x_j}$$

Where

The constant $\emptyset$ of the model is calculated by:

$$\emptyset = F_1\emptyset_1 + (1-F)\emptyset_2 \qquad \textit{Equation 5}$$

Eddy Viscosity

$$v_t = \frac{\alpha_1 k}{\max(\alpha_1\Omega;\ \Omega F_2)}$$

The Ω is the absolute value of the vorticity:

$$F_1 = tanh(ar\ g_1)\quad F_1 = tanh(ar\ g_2)\ \textit{Equation 6}$$

$$ar\ g_1 = \min\left[\max\left(\frac{\sqrt{k}}{0.09\omega y};\frac{500v}{y^2\omega}\right),\frac{3.424pk}{CD_{k\omega}y^2}\right], \quad ar\ g_2 = \max(2\frac{\sqrt{k}}{0.09\omega y};\frac{500v}{y^2\omega})$$

$$CD_{k\omega} = \max(1.712\rho\frac{1}{\omega}\frac{\partial k}{\partial k_j}\frac{\partial \omega}{\partial x_j}, 10^{-20}$$

3.3 Domain and the boundary conditions

The upstream velocity is fixed at 40 m/s, and the Reynolds number is 7.8 x 10^5 based on the height. Domain length is 5L (where L= car length of the model) at the rear of the model, and 2L at the front recommended by [18]. The cross-sectional dimension of the domain is 1.87m in width and 1.4m in height that provides a 4.3% blockage ratio similar to [19], which is used by [20]. For the body surface and floor, a no-slip boundary condition is used, and the roof and sidewalls are treated as slip walls [20]. Models are 50 mm above the ground, as kept in the original experiment [10]. A box of influence is created, which is 0.5L at the front and 1L at the rear end. It gives control to change the element characteristic inside and outside the box [21]. By using the symmetry condition, only half of the model is simulated to reduce time constraints, and the value of y^+ is controlled within 30 to 100. The initial 100 iterations are done by a first-order upwind discretization, which then switched to the second-order. A pressure-based coupled algorithm is used. Figure 4 shows the mesh.

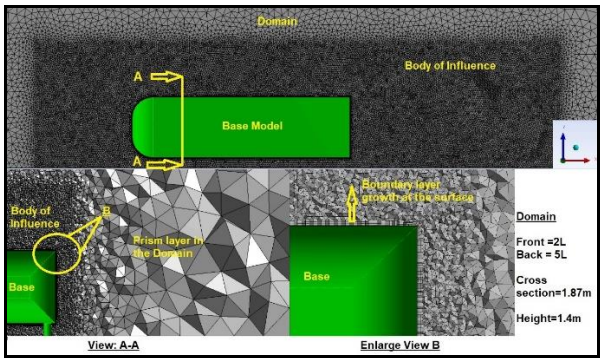

Figure 4 Details of the mesh

3.4 Validation

A grid independence study was conducted based on the drag coefficient. The element number was varied between 2.1 million for a coarse mesh to 13 million for a fine mesh. Thence, a medium-mesh with a 5mm element size contributing to 6.5 million elements was chosen based on a grid independence study for the simulation shown in Figure 5. The variation in the drag coefficient within these grid sizes was a maximum of 4.02% that is in the acceptable range.

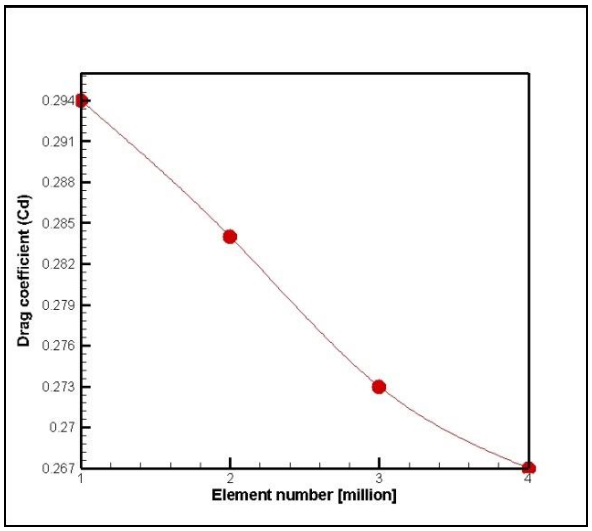

Figure 5 Grid independence study, where 1=2.1 Million, 2= 3.3 Million, 3 = 6.5 Million and 4=13 Million

The square back Ahmed body, the various drag coefficients are compared in Table 2. The slightly higher drag coefficient [22] stated that this value varies between 0.26 to 0.32 in the available literature, and hence the achieved drag coefficient for this particular case is similar to his experiment.

Table 2 Drag coefficient validation with the existing results for the square back Ahmed model

No.	Reference	Method	Drag coefficient	% Accuracy
1	(Ahmed et al., 1984)	Experiment	0.250	
2	(Grandemange et al., 2013)	Experiment	0.274	9.6
3	(Lucas et al., 2017)	Experiment	0.288	15.2
4	**Present study**	CFD Simulation	0.273	9.2

Also, the fractional bias (FB) of the present study $(2(\bar{u}_s+\bar{u}_e)$ is 0.2 considering the experimental values of [10], which is in the acceptable range of $-2 \leq FB \leq +2$ recommended by [23]. Where us is simulation velocity, and ue is the experimental value. Furthermore, one more important aspect of the flow topology at the base identified by several studies [24], [25], and others [22], [26] is the Torus shape vortex ring. This torus vortex is an important factor contributing to the pressure drop. The present simulation identified this torus vortex at the base shown in Figure 6. Such identification further highlights the correctness of the simulation.

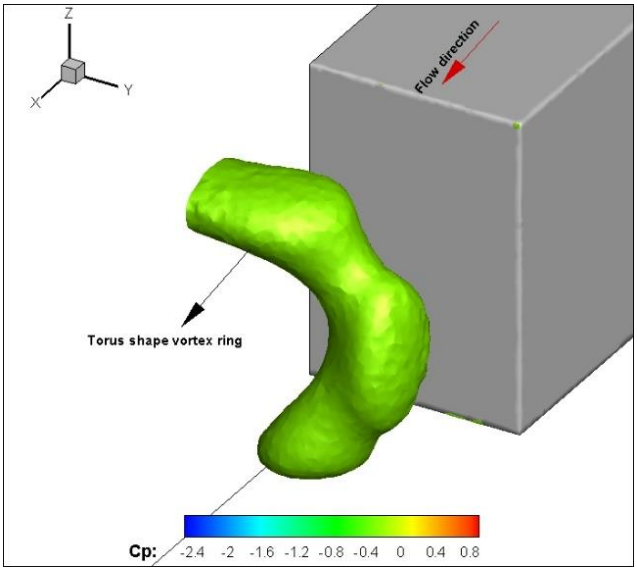

Figure 6 Torus ring vortex at the base of the base model.

4. Result and Discussion

As a dimensionless number, the drag coefficient denotes the drag force to dynamic pressure and projected area. The change in drag coefficient highlights the alterations made on the base model. There are four phases of this investigation on the base model. In the first phase, by implementing a rectangular plate (L=180mm, W=389mm) at the rear, the optimal flap angle (Maximum drag reduction) is investigated. As shown in Figure 7 (a), it was found to be 10° from the horizontal surface. In the second phase, at the optimal angle (10°), the length (L=180mm) of the flat plate was analyzed for the optimal length, shown in Figure 7(b). The optimized length was found to be 135mm which provides a further drag reduction. After optimizing the angle and length, the third phase attempted to find out the optimal width of the flap which is shown in Figure 7 (c) and resulted in 389mm. In the end, once an optimized length and width of the plate are found at a 10° angle, the effect of ground height was investigated between {25,100} depicted in Figure 7 (d). A ground height of 25mm gives the maximum drag reduction.

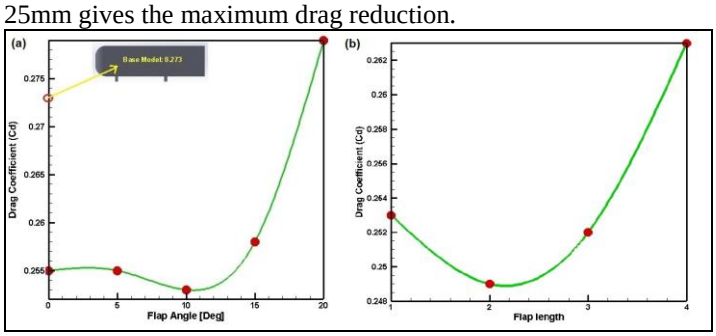

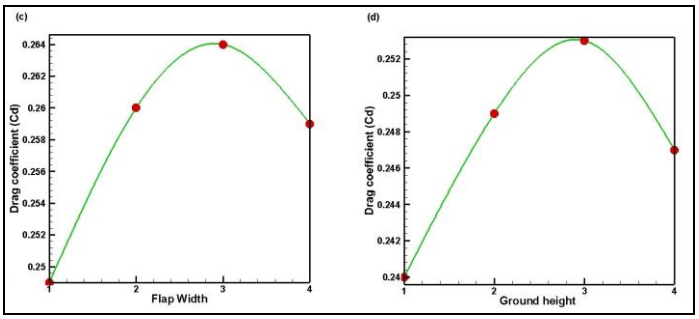

Figure 7 (a) The first phase: Drag coefficient versus flap angle (b) Second Phase: Drag coefficient versus flap length at constant optimized angle 10° where the X-axis represent, 1=10° Flap-1 =180mm, 2=10° Flap-2 =135mm, 3=10° Flap-3 =90mm and 4=10° Flap-4 =45mm (c) Third Phase: Drag coefficient versus flap width at optimized angle 10° and length 135mm where the X-axis represent, 1=10° Flap-1 =389mm, 2=10° Flap-2 =270mm, 3=10° Flap-3 =180mm and 4=10° Flap-4 =90mm (d) Fourth Phase: Drag coefficient versus ground height at optimized angle 10°, Length=135mm and width 389mm. where the X-axis represent, 1=Ground height 25, 2=Ground height 50mm, 3=Ground height 75mm and 4=Ground height 100mm

The first phase accentuates the critical role played by the angle. The role of the angle is highlighted by [5], [7], [27] for the slanted Ahmed body with flaps. However, [9] found the optimal angle for an elliptical flap to be 50° from the horizontal but on the contrary, [4] achieved a 20° optimal angle over a square back car. Furthermore, [28] found a 12° optimum angle over a square back Ahmed body with small flaps at the rear. Though all these cases are investigated over a blunt trailing edge, the reported maximum drag reduction differs significantly in terms of the implementation angle. In the absence of skin friction drag, the projected area remains the only parameter that influences the pressure drag. However, a study was conducted by [29] on the width to height aspect ratio over a fastback Ahmed body. It was found that increasing the width boosts the drag coefficient. Nonetheless, according to [30] as height to width-based aspect ratio decreases the drag coefficient decreases while experimenting on rectangular boxes. Therefore, it suggests the existence of a critical projected area for which the drag coefficient will be minimum. By ignoring this unknown projected area, the dynamics at the blunt edges of square back bodies suggest that the optimal angle for the flap is directly influenced by the front body flow topology. Furthermore, the influence of the side edge vortex is less significant in the square back model [31] which indicates that the recirculation region formed at the rear is the only distinguishing factor between the models. Though an independent comparative study is needed to validate and understand this problem, however, in the current case, a 10° angle provides the maximum drag reduction for a square back Ahmed model. While taking inspiration from [9] a 50° flap was simulated that did not provide any drag reduction (Cd=0.272).

The second phase studied the effect of flap length on the drag. A fine-tuned length of 135mm provides an increased drag reduction of 8.8% at a 10° angle. The influence of flap length

is explored by [2], [4], [5], [9], and others. For example, a boat-tail-like mechanism made of plates by Khalighi et al. [2] found 50mm length to be optimum, similarly,Capone et al. [4] reported 2/3H length which is 100mm, and [9] discovered it to be 120mm. The base model used in the above studies is different and hence, the optimized length also differs for the best drag reduction. Nonetheless, the only common thing between all these models is the application on the blunt edges. Similarly, except in the case of [2] where the plates are installed 8mm offset from the edges, both [4] and [9] matched the width of the flap with the base model. They did not attempt to see the effect of width on the pressure drag and hence the current investigation reveals that change (decrease) in the width at 135mm and 10° angle boosts the drag coefficient. It is found that the flap width that matched with the base model provides the maximum drag reduction. Therefore the aspect ratio of the flap has both incremental and detrimental effects. Where the length/width base aspect ratio has a specific aspect ratio (0.347) for the maximum drag reduction, the width/length aspect ratio has (2.88) at a 10° angle.

The effect of ground (height/ground) clearance directly influences the bottom vortex due to underbody flow [10]. The drag as a function of ground clearance is recently reported by Plumejeau et al. [32], Barros et al. [33]. A critical ground clearance of g/h=0.100 (where g is ground clearance and h is the model height) is reported by Plumejeau et al. [32] that provides the reduced pressure drag. The present work, reports huge drag reduction while altering the height as 25, 50,75 and 100mm for a 135mm flap at 10°. In such a case, at 25mm ground height, the flap further boosts the drag reduction to 12.5% compared to the base model. This height which is exactly half used by [10] proved to be more drag economical. Nonetheless, its practical use might be difficult due to necessary height requirement between vehicle and road for several other design considerations. However, a detailed investigation is needed for further understanding the precise change in the flow topology.

4.1 VORTEX IDENTIFICATION

The wake at the base is dominated by the vorticity-carrying-free-shear layer along with its vortical structure. The reason is attributed to the inviscid instability mechanism and to capture these structures, vortex identification methods are used [34], [35]. Two methods of identification are the most popular, the so-called Q-criterion proposed by Hunt [36] and Lambda ($\lambda 2$)-criterion given by Jeong et al. [37]. In the Q-criterion eddy is represented as the positive second invariant Q of the velocity gradient defined as $\frac{1}{2}(\|\boldsymbol{\Omega}^2\| - \|\mathbf{S}^2\|)$. Where $\boldsymbol{\Omega}^2$ and S^2 are symmetric and antisymmetric velocity divergence components. On the contrary, $\lambda 2$- criterion considers the second eigenvalue of the symmetric tensor $\mathbf{S}^2 + \boldsymbol{\Omega}^2$ capture the pressure minima.
Figure 8 and 9, shows the Q and $\lambda 2$ criterion respectively. Both these identification methods reveal the existence of a fully developed C-vortex when the flap is installed. However, such a matured C-vortex is absent in the base case which means that the major pressure minimums are inside the recirculation region vortex and hence, the base case shows a developed and long vortex.

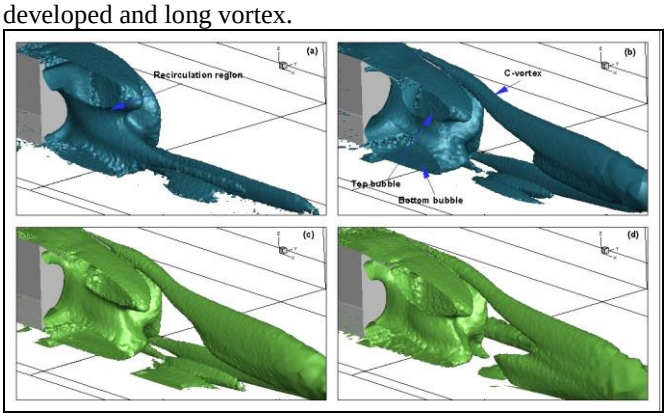

Figure 8 Q criterion of velocity invariant with Q=800 (a) base model without flap at ground height 50mm (b) Flap at 10° with 180mm length and 389 widths at ground height 50mm (c) Flap at 10° with 135mm length and 389mm width at ground height 50mm and (d) Flap at 10° with 135mm length and 389mm width at ground height 25mm

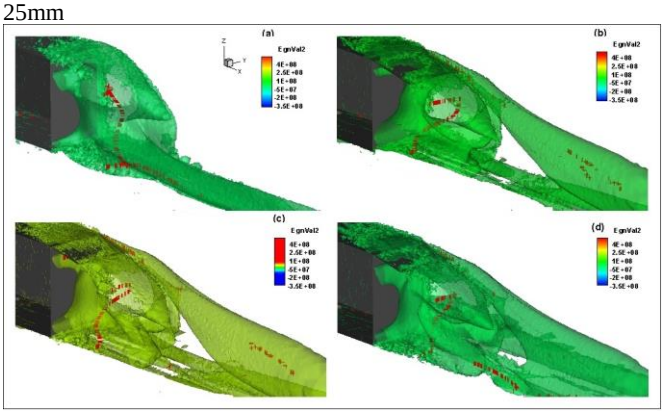

Figure 9 $\lambda 2$ criterion at Eignvalue=-450 (a) base model without flap at ground height 50mm (b) Flap at 10° with 180mm length and 389 widths at ground height 50mm (c) Flap at 10° with 135mm length and 389mm width at ground height 50mm and (d) Flap at 10° with 135mm length and 389mm width at ground height 25mm.

Installation of the flap at a 10° angle delays the separation by the length of the flap and then modifies the recirculation region as well. It creates two separate, top, and bottom bubbles but the size of the bottom bubble is quite large compared to the top. In the case of reduced ground height, the size of the bottom bubble is comparatively less. Hence, the flap transfers the momentum of the vortex to the region near the ground in all the cases with the flap. Furthermore, Figure 9 also shows the Vortex core location in red lines which further explains that in the base case Figure 9(a), the vortex core location remains in the recirculation region but with the flap, it consists of C-vortex, top bubble, bottom bubble and the underbody vortex going into the downstream direction.

5 CONCLUSION

An investigation has been made over a square back Ahmed body drag reduction using a simple passive flap device. Three important parameters were examined namely, the angle of implementation, length, and width of the flap. It was found that the 10° angle shows the least drag reduction. Similarly, the length also plays a critical role, and at 135mm length placed at 10° provides the 8.7% drag reduction. However, a decrease in width increases the drag which is quite remarkable. Furthermore, the vortex identification methods demonstrate that the flap delays the separation and creates two bubbles at the vertical base. Therefore, such understanding provides avenues to invent new flow control devices to alter the bubbles along with the flap.

REFERENCE

[1] W. R. Lanser, J. C. Ross, and A. E. Kaufman, "Aerodynamic Performance of a Drag Reduction Device on a Full-Scale Tractor/Trailer," Sep. 1991, doi: 10.4271/912125.

[2] B. Khalighi *et al.*, "Experimental and computational study of unsteady wake flow behind a bluff body with a drag reduction device," in *SAE Technical Papers*, Mar. 2001, doi: 10.4271/2001-01-1042.

[3] S. R. Balkanyi, L. P. Bernal, and B. Khalighi, "Analysis of the near wake of bluff bodies in ground proximity," in *ASME International Mechanical Engineering Congress and Exposition, Proceedings*, Jun. 2002, pp. 705–713, doi: 10.1115/IMECE2002-32347.

[4] A. Capone and G. P. Romano, "Investigation on the effect of horizontal and vertical deflectors on the near-wake of a square-back car model," *J. Wind Eng. Ind. Aerodyn.*, vol. 185, pp. 57–64, Feb. 2019, doi: 10.1016/j.jweia.2018.12.011.

[5] J.-F. Beaudoin and J.-L. Aider, "Drag and lift reduction of a 3D bluff body using flaps," *Exp. Fluids*, vol. 44, no. 4, pp. 491–501, Apr. 2008, doi: 10.1007/s00348-007-0392-1.

[6] G. Fourrié, L. Keirsbulck, L. Labraga, and P. Gilliéron, "Bluff-body drag reduction using a deflector," *Exp. Fluids*, vol. 50, no. 2, pp. 385–395, Feb. 2011, doi: 10.1007/s00348-010-0937-6.

[7] J. Tian, Y. Zhang, H. Zhu, and H. Xiao, "Aerodynamic drag reduction and flow control of Ahmed body with flaps," *Adv. Mech. Eng.*, vol. 9, no. 7, pp. 1–17, 2017, doi: 10.1177/1687814017711390.

[8] D. Kim, H. Lee, W. Yi, and H. Choi, "A bio-inspired device for drag reduction on a three-dimensional model vehicle," *Bioinspir. Biomim.*, vol. 11, no. 2, p. 026004, Mar. 2016, doi: 10.1088/1748-3190/11/2/026004.

[9] A. Altaf, A. A. Omar, and W. Asrar, "Passive drag reduction of square back road vehicles," *Jnl. Wind Eng. Ind. Aerodyn.*, vol. 134, pp. 30–43, 2014, doi: 10.1016/j.jweia.2014.08.006.

[10] S. R. Ahmed, G. Ramm, and G. Faltin, "Some Salient Features Of The Time-Averaged Ground Vehicle Wake," *SAE Trans.*, vol. 93, no. 2, pp. 473–503, Feb. 1984, doi: 10.4271/840300.

[11] Y. Egorov and F. Menter, "Development and Application of SST-SAS Turbulence Model in the DESIDER Project Outline • Scale-Adaptive Simulation (SAS) concept • SST-SAS turbulence model • Aerodynamic applications – NACA0021 airfoil beyond stall – Delta wing – Full aircraft configura," pp. 1–23, 2007.

[12] S.-E. Kim, S. Mathur, J. Murthy, and D. Choudhury, "A Reynolds-averaged Navier-Stokes solver using unstructured mesh-based finite-volume scheme," in *36th AIAA Aerospace Sciences Meeting and Exhibit*, Jan. 1998, doi: 10.2514/6.1998-231.

[13] P. Taylor and F. R. Menter, "Review of the shear-stress transport turbulence model experience from an industrial perspective," *Int. J. Comut. Fluid Dyn.*, no. January 2013, pp. 37–41, 2009, doi: 10.1080/10618560902773387.

[14] M. Corallo, J. Sheridan, and M. C. Thompson, "Effect of aspect ratio on the near-wake flow structure of an Ahmed body," *Jnl. Wind Eng. Ind. Aerodyn.*, vol. 147, pp. 95–103, 2015, doi: 10.1016/j.jweia.2015.09.006.

[15] F. R. Menter, M. Kuntz, and R. Langtry, "Ten Years of Industrial Experience with the SST Turbulence Model," 2003.

[16] F. R. Menter, "Two-equation eddy-viscosity turbulence models for engineering applications," *AIAA J.*, vol. 32, no. 8, pp. 1598–1605, 1994, doi: 10.2514/3.12149.

[17] D. Igali, O. Mukhmetov, Y. Zhao, S. C. Fok, and S. L. Teh, "Comparative Analysis of Turbulence Models for Automotive Aerodynamic Simulation and Design," *Int. J. Automot. Technol.*, vol. 20, no. 6, pp. 1145–1152, Dec. 2019, doi: 10.1007/s12239-019-0107-7.

[18] R. Manceau and J.Bonnet, Eds., "10th joint ERCOFTAC/IAHR/QNET-CFD Workshop on Refined Turbulence Modelling," 2002.

[19] H. Lienhart, C. Stoots, and S. Becker, "Flow and Turbulence Structures in the Wake of a Simplified Car Model (Ahmed Modell)," in *New Results in Numerical and Experimental Fluid Mechanics III*, Springer Berlin Heidelberg, 2002, pp. 323–330.

[20] E. Guilmineau, G. Deng, and J. Wackers, "Numerical simulation with a DES approach for automotive flows," *J. Fluids Struct.*, vol. 27, no. 5–6, pp. 807–816, Jul. 2011, doi: 10.1016/J.JFLUIDSTRUCTS.2011.03.010.

[21] M. Lanfrit, "Best practice guidelines for handling Automotive External Aerodynamics with FLUENT," 2005.

[22] M. Grandemange, M. Gohlke, and O. Cadot, "Turbulent wake past a three-dimensional blunt body. Part 1. Global modes and bi-stability," *J. Fluid Mech.*, vol. 722, pp. 51–84, May 2013, doi: 10.1017/jfm.2013.83.

[23] C. Emery, Z. Liu, A. G. Russell, M. T. Odman, G. Yarwood, and N. Kumar, "Recommendations on statistics and benchmarks to assess photochemical model performance," *J. Air Waste Manage. Assoc.*, vol. 67, no. 5, pp. 582–598, Apr. 2017, doi: 10.1080/10962247.2016.1265027.

[24] S. Krajnović and L. Davidson, "Numerical study of the flow around a bus-shaped body," *J. Fluids Eng. Trans. ASME*, vol. 125, no. 3, pp. 500–509, May 2003, doi: 10.1115/1.1567305.

[25] J.-M. Lucas, O. Cadot, V. Herbert, S. Parpais, and J. Délery, "A numerical investigation of the asymmetric wake mode of a squareback Ahmed body – effect of a base cavity," *J. Fluid Mech.*, vol. 831, pp. 675–697, Nov. 2017, doi: 10.1017/jfm.2017.654.

[26] M. Rouméas, P. Gilliéron, and A. Kourta, "Analysis and control of the near-wake flow over a square-back geometry," *Comput. Fluids*, vol. 38, no. 1, pp. 60–70, Jan. 2009, doi: 10.1016/j.compfluid.2008.01.009.

[27] G. Fourrié, L. Keirsbulck, L. Labraga, and P. Gilliéron, "Bluff-body drag reduction using a deflector," *Exp. Fluids*, vol. 50, no. 2, pp. 385–395, Feb. 2011, doi: 10.1007/s00348-010-0937-6.

[28] Y. Eulalie, P. Gilotte, and I. Mortazavi, "Numerical study of flow control strategies for a simplified square back ground vehicle," *Fluid Dyn. Res.*, vol. 49, no. 3, Mar. 2017, doi: 10.1088/1873-7005/aa5c54.

[29] M. Corallo, J. Sheridan, and M. C. Thompson, "Effect of aspect ratio on the near-wake flow structure of an Ahmed body," *J. Wind Eng. Ind. Aerodyn.*, vol. 147, pp. 95–103, Dec. 2015, doi: 10.1016/J.JWEIA.2015.09.006.

[30] J. Williams, J. Barlow, and R. Ranzenbach, "Experimental Study of C D Variation With Aspect Ratio," Michigan, 1999.

[31] D. E. Aljure, O. Lehmkuhl, I. Rodríguez, and A. Oliva, "Flow and turbulent structures around simplified car models," *Comput. Fluids*, vol. 96, pp. 122–135, Jun. 2014, doi: 10.1016/j.compfluid.2014.03.013.

[32] B. Plumejeau, L. Keirsbulck, S. Delprat, M. Lippert, and W. Abassi, "Behavior of the square-back Ahmed body global modes at low ground clearance," *Phys. Rev. Fluids*, vol. 5, no. 8, p. 084701, Aug. 2020, doi: 10.1103/physrevfluids.5.084701.

[33] D. Barros, J. Borée, O. Cadot, A. Spohn, and B. R. Noack, "Forcing symmetry exchanges and flow reversals in turbulent wakes," *J. Fluid Mech.*, vol. 829, Oct. 2017, doi: 10.1017/jfm.2017.590.

[34] B. R. McAuliffe and M. I. Yaras, "Numerical study of instability mechanisms leading to transition in separation bubbles," *J. Turbomach.*, vol. 130, no. 2, Apr. 2008, doi: 10.1115/1.2750680.

[35] U. Caylan, "Computations and Measurements of the Effects of Trailing-Edge Geometry on the Wake of Bluff Bodies," 2019.

[36] J. C. R. Hunt, A. A. Wray, and P. Moin, "Eddies, streams, and convergence zones in turbulent flows." 1988, Accessed: Jul. 19, 2019. [Online]. Available: https://www.semanticscholar.org/paper/Eddies%2C-streams%2C-and-convergence-zones-in-turbulent-Hunt-Wray/4e1d2fdcd44cc416e44b6186c1f7c23cc1200b7c.

[37] J. Jeong and F. Hussain, "On the identification of a vortex," *J. Fluid Mech.*, vol. 285, no. 1, p. 69, Feb. 1995, doi: 10.1017/S0022112095000462.